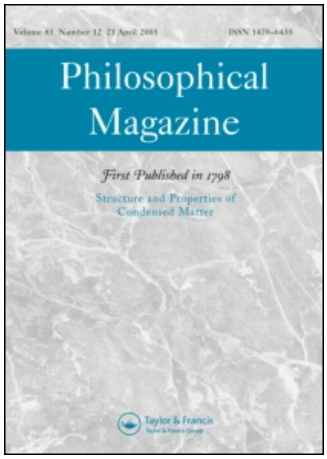

Philosophical Magazine
First published in 1798
Publication details, including instructions for authors and subscription information:
http://www.informaworld.com/smpp/title~content=t713695589

Localization of excitation in InGaN epilayers

To cite this Article: , 'Localization of excitation in InGaN epilayers', Philosophical Magazine, 87:13, 1999 - 2017
To link to this article: DOI: 10.1080/14786430701342164
URL: http://dx.doi.org/10.1080/14786430701342164

Philosophical Magazine,
Vol. 87, No. 13, 1 May 2007, 1999–2017

Localization of excitation in InGaN epilayers

V. KACHKANOV†, K. P. O'DONNELL*†, S. PEREIRA‡ and R. W. MARTIN†

†SUPA, Department of Physics, University of Strathclyde,
Glasgow G4 0NG, UK
‡CICECO and Departamento de Fisica, Universidade de Aveiro,
Aveiro, Portugal

(*Received 3 July 2006; accepted in revised form 9 March 2007*)

Energy scalability of the excitation–emission spectra of InGaN epilayers, quantum wells and light-emitting diodes provided indirect evidence for a fundamental common cause of the remarkable optical properties of this commercially important semiconductor alloy. Phase segregation on the nanoscale (accidental quantum dot formation) has generally been accepted as the mechanism of the spectral energy scaling (K.P. O'Donnell, R.W. Martin and P.G. Middleton, Phys. Rev. Lett. **82** 237 (1999)). Recently, however, the downsizing of the InN bandgap, from 2 to about 1 eV, has prompted a re-examination of the observations. Here, we present new structural evidence of InGaN nanostructure, obtained from a comparative analysis of Ga and In K-edge EXAFS (extended X-ray absorption fine structure) of a wide range of $In_xGa_{1-x}N$ epilayer samples. The mean In–Ga and Ga–In next-nearest-neighbour (NNN) separations are found to be unequal in length for InN-poor ($0.1 < x < 0.4$) samples. The degree of inequality *increases* with *decreasing* InN fraction, x, and therefore correlates with luminescence efficiency in this range of alloy composition. We propose that the breakdown of In/Ga randomicity in InGaN alloys is associated with efficient excitation–emission in blue-green light-emitting devices. Although non-randomicity may lead to a weak quasi-localization of excitation, through the suppression of energy back-transfer, the issue of strong exciton localization in InGaN is not directly addressed by these results.

1. Introduction

Localization of excitons by phase segregation [1] is routinely invoked to explain the high efficiency of InGaN luminescent devices in the face of defect densities much larger than those encountered in other semiconductor materials. The most convincing evidence in support of a correlated spatial and energy localization of excitons is the micro-spectroscopic observation of a characteristic "spotty"

*Corresponding author. Email: k.p.odonnell@strath.ac.uk

Philosophical Magazine
ISSN 1478–6435 print/ISSN 1478–6443 online © 2007 Taylor & Francis
http://www.tandf.co.uk/journals
DOI: 10.1080/14786430701342164

luminescence texture with a length scale of order 100 nm in PL and CL micrographs of InGaN epilayers [2].

While electron–hole localization is widely accepted as a key to enhanced luminescence efficiency in solids, the origin of the localization mechanism in InGaN is a matter of continuing dispute. Self-formed or 'accidental' InN quantum dots [3, 4] or In-rich (properly, InN-rich) InGaN clusters [5, 6] may act as centres for exciton localization. However, the discovery of the narrow band gap of InN, recently downsized from 2 to about 1 eV [7], makes it less likely that pure InN quantum dots can be solely responsible for InGaN luminescence, since quantum confinement in these structures would have to be very strong to upshift the emission energy by $\sim$2 eV from the InN band edge to the visible spectral region at which device efficiencies are maximized: pure InN dots with emission near 3 eV necessarily contain only a few In atoms. In experimental terms, the problem of identifying the nanoscale structure of such poorly defined lumophores (''quantum whats'') with particular spectral features is very challenging, while the calculation of the spectral signatures of exemplars may lie beyond present theoretical capabilities. Moreover, it is quite difficult to imagine how assemblies (menageries) of small lattice animals with narrow spectral signatures, similar to those identified in spatially resolved photoluminescence experiments [8], can give rise to a seemingly continuous range of emission energies.

Transmission electron microscopy (TEM) [5] and energy dispersive X-ray (EDX) imaging of InGaN quantum wells (QW) [6] have claimed to reveal InN-rich clusters, embedded in wells, as distinct contrast spots with a characteristic size of about 3 nm. (Other contributors to this issue will no doubt provide further instances of such observations.) However, both TEM and EDX techniques involve exposure of samples to high-energy ($\sim$100 keV) electron bombardment, which may by itself induce phase separation in alloys [9, 10]. X-ray diffraction (XRD) is another experimental technique that can provide information about phase segregation, if carefully applied. Many authors have reported double (or some higher multiple) XRD peaks in θ–2θ scans, and doublet luminescence peaks in emission spectra, of InGaN epilayers on GaN [11, 12]. These observations were casually ascribed to InN clustering [13], but it has since been shown that the attribution of distinct diffraction peaks to separated phases depends upon an incorrect application of Vegard's law which does not take into account the strain state of samples [14]. The joint observation of a luminescence doublet and a split XRD peak can often be better explained by the coexistence of *two* InGaN layers with the *same* InN fraction but *different* states of strain: one layer at the sample surface is relaxed while the other lies close to the GaN substrate, almost coherent with it [15, 16]. The so-called ''S-shape'' of the temperature dependence of the emission peak of InGaN samples has also been described in terms of thermal redistribution of excitons among centres with a range of localization energies [17]. In certain cases, however, an S-shaped dependence will arise naturally if an unresolved luminescence doublet of the kind described above has components with very different temperature dependences (unpublished data).

We conclude from the above brief summary that, despite nearly ten years of effort, no uncontested evidence of a relation between InN–GaN phase segregation

and enhanced luminescence efficiency of InGaN has been obtained in any laboratory. But phase segregation should lead to a characteristic non-randomness in the distribution of cations in a common-anion pseudobinary alloy, and we should exploit experimental techniques that can reveal this. Extended X-ray absorption fine structure (EXAFS) analysis provides a unique structural tool for the acquisition of information about the atomic environment of specific elements in a solid, the so-called local structure [18]. EXAFS is a modulation of the absorption coefficient above a characteristic X-ray absorption edge of the ''target'' atomic species. It results from the scattering of ejected photoelectrons by atoms in the immediate neighbourhood and their subsequent interference with the outgoing photoelectron wave. EXAFS analysis reveals the chemical nature and coordination number of the surrounding atoms and their radial separation from the central absorber.

Although it provides information about atomic interactions on a sub-nanometre scale, EXAFS is not a microscopic technique. Microscopies (such as TEM) provide top–down analysis, limited by issues of magnification and resolution, whereas EXAFS offers a bottom-up approach. EXAFS tells us about chemical bonding, coordination numbers, bond lengths and so on, working from the nearest to the next nearest neighbours (NNN) and beyond, to build up a ''picture'' of the average environment of a chosen atomic species in a sample. It is limited by the fact that more distant neighbours interact more weakly with the ejected photoelectron and are therefore less visible. In other words, EXAFS provides statistical information about the first few moments of the spatial distribution of near neighbours to a targeted atomic species, e.g. Ga or In, in a solid.

Consider, by way of a guiding example, a ''non-random alloy'' to be formed artificially by gluing a sample of InN to an equal one of GaN. Although the InN fraction of this (very odd) sample will be exactly 50%, EXAFS on the In sublattice will reveal only In atoms in NNN positions, whereas Ga atoms would have all-Ga NNN, according to EXAFS. The degree of phase segregation in such a sample would be estimated as total. Obviously, many other distributions of cation locations could provide the same statistical result within experimental error.

In this contribution we present the first direct measurement of the degree of phase segregation in InGaN alloys from a detailed analysis that compares the In and Ga local environments for the complete range of $In_xGa_{1-x}N$ alloys accessible to the EXAFS technique (roughly $0.1 < x < 0.9$). We then attempt to relate this statistical-structural information to the well-known luminescence properties of InGaN alloy.

2. Samples and experimental details

$In_xGa_{1-x}N$ samples were grown either by molecular beam epitaxy (MBE) or by metal–organic chemical vapour deposition (MOCVD). MBE samples with ''low'' InN contents ($x < 0.40$), and all of the MOCVD samples ($0.1 < x \leq 0.4$), included an InGaN epilayer, some 200–500 nm thick, grown on a 1–2 μm thick GaN buffer layer on sapphire. InN-rich MBE samples ($x \geq 0.60$) were grown directly on sapphire substrates without any buffer layers. The In/Ga ratio of all layers was measured

using wavelength dispersive X-ray (WDX) analysis in a Cameca SX100 Electron Probe Micro-Analyser (EPMA). The intensities of characteristic X-ray emissions from In and Ga in the samples were compared with those from InAs (or InP) and GaN standards [19].

EXAFS spectra were measured on stations 7.1 and 16.5 of the UK Synchrotron Radiation Source (SRS) at Daresbury Laboratory. The local structure of In and Ga atoms in InGaN epilayers was probed by means of In K-edge (27 928 eV, station 16.5) and Ga K-edge (10 370 eV, station 7.1) EXAFS measured in fluorescence (FLY) and total electron yield (TEY) modes. On station 7.1, a Si(111) double-crystal monochromator, with sagittally bent second crystal, and a nine-element monolithic Ge detector were used to measure EXAFS spectra. A Si(200) double-crystal monochromator along with a 30-element solid-state Ge detector were used to collect EXAFS data on station 16.5. EXAFS measurements in TEY mode were performed in a chamber filled with helium. A Keithley 427 amplifier was used to detect current associated with X-ray absorption. TEY probes a thin layer (~5 nm) close to the sample surface and was chosen for the detection of Ga K-edge absorption in order to avoid any contribution to the InGaN EXAFS signal from Ga atoms located in the buffer. FLY and TEY In K-edge EXAFS was also measured to investigate the possibility of surface segregation. Interatomic distances obtained from the In K-edge EXAFS of InGaN measured in TEY and FLY modes were found to be identical within the measurement error: this preliminary result shows that there are no significant structural differences on a local scale between the bulk of samples and thin layers close to the surface. Therefore, in what follows, In local structure parameters obtained by In K-edge FLY EXAFS will be compared with Ga local structure parameters obtained by Ga K-edge TEY EXAFS. The local structure parameters of MBE- and MOCVD-grown InGaN epilayers are shown in tables 1 and 2, respectively.

The model of the local structure used to simulate In or Ga EXAFS was restricted to the two closest atomic coordination spheres that are of greatest interest. (This model is simpler than that used by Blant *et al.* [20] and more reliable, since the contribution to EXAFS from nitrogen atoms in the third coordination sphere is rather weak and hard to resolve). The first coordination sphere always comprised four nitrogen atoms. The second coordination sphere was a mixture of In and Ga atoms, with the total number of atoms fixed at 12. The In–In, Ga–Ga, In–Ga and Ga–In distances were refined separately. The ratio of cationic species (In to Ga) in the second coordination sphere was also varied during the fitting procedure to best fit the experimental EXAFS. This ratio serves as a useful check of self-consistency with the independently measured In/Ga ratio obtained by EPMA. The fit quality was examined using the fit index R, which is defined by the expression:

$$R = \sum_i \left[\left(\frac{1}{(\sigma_i)} \right) \left(\left| \text{experiment}(i) - \text{theory}(i) \right| \right) \right] \times 100\%, \qquad (1)$$

Table 1. Local structure parameters for MBE grown InGaN epilayers.

InN content, %	Element and detection mode	Atom type	Number of atoms	Distance, Å	Debye–Waller factor, Å	k range, Å^{-1}	Fit index R
100	In K-edge FLY	N	4	2.15 ± 0.02	0.007	2–15	29.30
		In	12	3.52 ± 0.01	0.013		
96.3	In K-edge FLY	N	4	2.15 ± 0.02	0.006	2–11	28.78
		In	12	3.52 ± 0.01	0.014		
77.8	In K-edge FLY	N	4	2.14 ± 0.02	0.010	1.5–11	30.69
		Ga	3.4 ± 1.0	3.41 ± 0.05	0.021		
		In	8.6 ± 1.0	3.45 ± 0.02	0.021		
	In K-edge TEY	N	4	2.12 ± 0.02	0.015	1.7–11	43.90
		Ga	4.0 ± 1.8	3.39 ± 0.06	0.023		
		In	8.0 ± 1.8	3.44 ± 0.02	0.023		
	Ga K-edge TEY	N	4	1.98 ± 0.02	0.014	2.5–13	35.94
		Ga	3.1 ± 1.8	3.31 ± 0.07	0.023		
		In	8.9 ± 1.8	3.42 ± 0.03	0.023		
60.1	In K-edge FLY	N	4	2.13 ± 0.01	0.010	2–11	30.58
		Ga	4.3 ± 0.9	3.37 ± 0.02	0.017		
		In	7.7 ± 0.9	3.43 ± 0.01	0.017		
	In K-edge TEY	N	4	2.13 ± 0.01	0.006	2–11	29.78
		Ga	4.0 ± 0.6	3.38 ± 0.03	0.017		
		In	8.0 ± 0.6	3.42 ± 0.01	0.017		
	Ga K-edge TEY	N	4	1.97 ± 0.02	0.016	2.5–11	38.37
		Ga	6.0 ± 1.3	3.30 ± 0.03	0.020		
		In	6.0 ± 1.3	3.36 ± 0.03	0.020		
34.9	In K-edge FLY	N	4	2.10 ± 0.01	0.006	1.7–11	34.20
		Ga	7.0 ± 0.8	3.30 ± 0.02	0.017		
		In	5.0 ± 0.8	3.32 ± 0.03	0.017		
	Ga K-edge TEY	N	4	1.93 ± 0.01	0.004	2.5–13	27.08
		Ga	9.4 ± 0.7	3.21 ± 0.01	0.015		
		In	2.6 ± 0.7	3.24 ± 0.03	0.015		
27.3	In K-edge FLY	N	4	2.09 ± 0.02	0.005	1.8–11	33.61
		Ga	8.1 ± 0.9	3.28 ± 0.02	0.018		
		In	3.9 ± 0.9	3.32 ± 0.03	0.018		
	In K-edge TEY	N	4	2.08 ± 0.02	0.014	1.7–10.5	42.48
		Ga	9.2 ± 1.8	3.26 ± 0.02	0.019		
		In	2.8 ± 1.8	3.33 ± 0.09	0.019		
	Ga K-edge TEY	N	4	1.94 ± 0.01	0.006	2.5–13	31.39
		Ga	9.4 ± 1.1	3.19 ± 0.01	0.015		
		In	2.6 ± 1.1	3.19 ± 0.03	0.015		

(*continued*)

Table 1. Continued.

InN content, %	Element and detection mode	Atom type	Number of atoms	Distance, Å	Debye–Waller factor, Å	k range, Å^{-1}	Fit index R
26.8	In K-edge FLY	N	4	2.10 ± 0.01	0.006	1.7–11	27.89
		Ga	8.0 ± 0.9	3.27 ± 0.02	0.017		
		In	4.0 ± 0.9	3.31 ± 0.02	0.017		
	In K-edge TEY	N	4	2.08 ± 0.02	0.009	2–11	41.59
		Ga	9.3 ± 1.7	3.27 ± 0.03	0.024		
		In	2.7 ± 1.7	3.33 ± 0.08	0.024		
	Ga K-edge TEY	N	4	1.94 ± 0.02	0.011	2.5–12	33.33
		Ga	9.8 ± 1.0	3.18 ± 0.02	0.013		
		In	2.2 ± 1.0	3.21 ± 0.06	0.013		
23.3	In K-edge FLY	N	4	2.08 ± 0.02	0.005	1.5–11	36.92
		Ga	10.3 ± 1.5	3.27 ± 0.02	0.023		
		In	1.7 ± 1.5	3.30 ± 0.07	0.023		
	In K-edge TEY	N	4	2.07 ± 0.01	0.014	1.7–10	38.94
		Ga	10.6 ± 1.2	3.25 ± 0.02	0.022		
		In	1.4 ± 1.2	3.30 ± 0.30	0.022		
	Ga K-edge TEY	N	4	1.94 ± 0.03	0.003	2.5–13	37.25
		Ga	8.9 ± 0.2	3.20 ± 0.01	0.007		
		In	3.1 ± 0.2	3.20 ± 0.02	0.007		
13.5	In K-edge FLY	N	4	2.08 ± 0.02	0.012	1.5–11	47.00
		Ga	12	3.25 ± 0.02	0.024		
	Ga K-edge TEY	N	4	1.93 ± 0.02	0.008	2.5–13	34.42
		Ga	12	3.18 ± 0.01	0.015		

where $1/(\sigma_i) = [k(i)]^2/\left(\sum_i [k(i)]^2 \left|\text{experiment}(i)\right|\right)$. The validity of extra parameters for each EXAFS simulation was checked using a reduced χ^2 method:

$$\text{reduced } \chi^2 = \frac{1}{(N_i - N_v)} \sum_i^N \left(\frac{X_{\text{data}}(k_i) - X_{\text{model}}(k_i)}{\varepsilon_i} \right)^2, \tag{2}$$

where ε_i is the uncertainty at each point (assumed to be the same at each point), X_{data} and X_{model} are the experimental and model values of the EXAFS at the same point, N_i is the number of independent points and N_v is the number of variables used in the fitting. Since in the *reduced* χ^2 test, the assumption is made that the uncertainty is the same at each point, the values of *reduced* χ^2 were used for comparison of competing models only. The difference in the parameter values between the best-fit value and the value for which the fit index was increased by 5% served as an estimate of the fitting error. The representative EXAFS spectra and their Fourier transforms along with simulated data are shown in figure 1.

High-resolution XRD characterization was performed on selected samples using a double-crystal diffractometer. The instrumental angular resolution is about 30 seconds of arc. A flat Ge (444) monochromator and horizontal divergence slits

Table 2. Local structure parameters for InGaN samples grown by MOCVD.

InN content, %	Element and detection mode	Atom type	Number of atoms	Distance, Å	Debye–Waller factor, Å^2	k range, Å^{-1}	Fit index R
40	In K-edge FLY	N	4	2.12 ± 0.01	0.007	1.5–11	25.12
		Ga	7.2 ± 0.6	3.31 ± 0.02	0.018		
		In	4.8 ± 0.6	3.37 ± 0.02	0.018		
	In K-edge TEY	N	4	2.11 ± 0.01	0.006	2–12	40.20
		Ga	6.7 ± 1.7	3.33 ± 0.03	0.020		
		In	5.3 ± 1.7	3.39 ± 0.03	0.020		
	Ga K-edge TEY	N	4	1.95 ± 0.03	0.003	2.5–11	33.73
		Ga	8.1 ± 1.2	3.24 ± 0.01	0.013		
		In	3.9 ± 1.2	3.31 ± 0.03	0.013		
35	In K-edge FLY	N	4	2.12 ± 0.01	0.008	1.5–11	28.05
		Ga	8.0 ± 0.8	3.30 ± 0.02	0.019		
		In	4.0 ± 0.8	3.35 ± 0.03	0.019		
	In K-edge TEY	N	4	2.12 ± 0.01	0.008	2–10.5	40.97
		Ga	7.1 ± 2.0	3.31 ± 0.04	0.022		
		In	4.9 ± 2.0	3.35 ± 0.03	0.022		
	Ga K-edge TEY	N	4	1.95 ± 0.01	0.008	2.5–11	24.73
		Ga	8.7 ± 0.8	3.25 ± 0.02	0.015		
		In	3.3 ± 0.8	3.27 ± 0.03	0.015		
27	In K-edge FLY	N	4	2.11 ± 0.01	0.008	1.5–11	27.98
		Ga	8.1 ± 0.7	3.29 ± 0.02	0.017		
		In	3.9 ± 0.7	3.35 ± 0.02	0.017		
	In K-edge TEY	N	4	2.09 ± 0.02	0.010	2–10.5	36.77
		Ga	9.0 ± 2.3	3.28 ± 0.04	0.024		
		In	3.0 ± 2.3	3.31 ± 0.08	0.024		
	Ga K-edge TEY	N	4	1.95 ± 0.02	0.010	2.5–12	31
		Ga	9.1 ± 0.6	3.23 ± 0.01	0.012		
		In	2.9 ± 0.6	3.24 ± 0.02	0.012		
24	In K-edge FLY	N	4	2.09 ± 0.01	0.004	1.5–11	33.57
		Ga	8.6 ± 1.3	3.27 ± 0.02	0.021		
		In	3.4 ± 1.3	3.33 ± 0.06	0.021		
	In K-edge TEY	N	4	2.07 ± 0.03	0.027	1.7–12	57.74
		Ga	9.4 ± 2.2	3.27 ± 0.03	0.021		
		In	2.6 ± 2.2	3.31 ± 0.06	0.007		
	Ga K-edge TEY	N	4	1.95 ± 0.02	0.010	2.5–12.5	28.89
		Ga	9.8 ± 0.7	3.21 ± 0.01	0.012		
		In	2.2 ± 0.7	3.21 ± 0.03	0.012		
10.5	In K-edge FLY	N	4	2.10 ± 0.01	0.005	1.5–11	31.35
		Ga	12	3.23 ± 0.02	0.013		
	Ga K-edge TEY	N	4	1.94 ± 0.02	0.004	2.5–13	37.31
		Ga	12	3.18 ± 0.02	0.013		

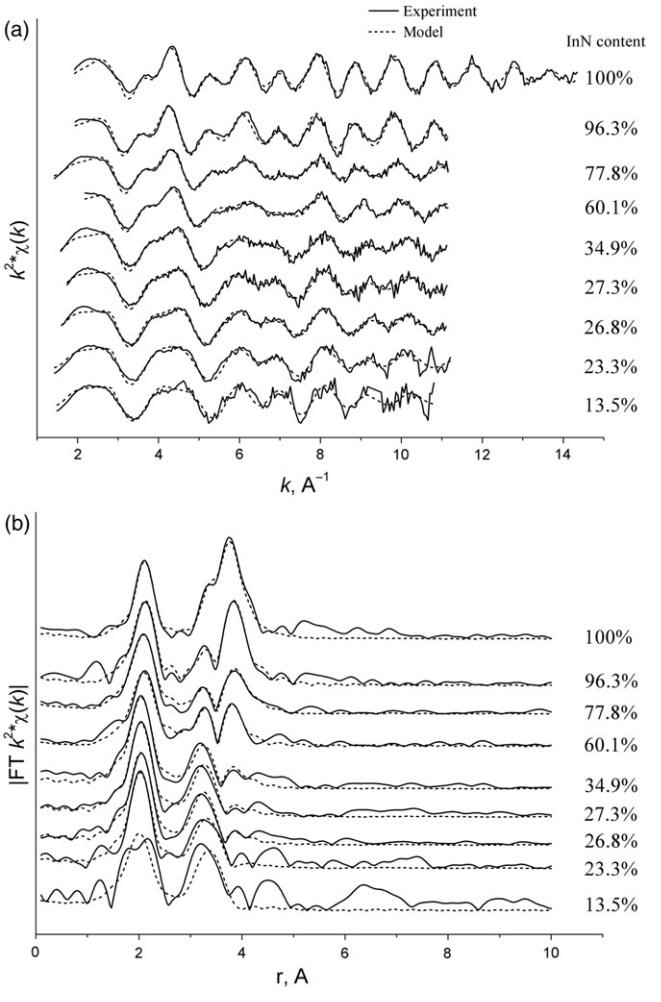

Figure 1. k^2-weighted In K-edge FLY EXAFS (a) and their Fourier transform moduli (b) for MBE InGaN epilayers.

with widths of 100 m and a height of 2 mm were used to select Cu K_{α_1} radiation. A position sensitive detector was placed at a variable distance from the sample in an achromatic geometry.

3. Results and discussion

3.1. *EXAFS analysis*

Mikkelsen and Boyce (MB hereafter) were first to apply EXAFS to local structural studies of semiconductor solid solutions [21]. They discovered that the nearest

neighbour (NN) bond lengths in InGaAs, i.e. In–As and Ga–As, are similar in magnitude to those of the binary constituents InAs and GaAs, respectively, but that the *weighted average* of In–As and Ga–As bond lengths in InGaAs follows Vegard's law. The bimodal distribution of NN bonds and their weak dependence on composition is probably a universal property of pseudobinary alloys [22]; it has also been observed in GaAsP [23], CdMnTe [24] and ZnMnSe [25]. Concerning the next-nearest neighbour (NNN) separations, i.e. the cation–cation distances, MB noted that in the absence of clustering, the In–Ga separation (obtained from In-edge EXAFS) and the Ga–In separation (obtained from Ga-edge EXAFS) agree with each other very closely throughout the whole composition range of InGaAs alloys. These distances were also found to be closely comparable to the lattice constant, a, of the alloys that were obtained from X-ray diffraction (XRD) measurements which exemplified Vegard's law.

The In–N and Ga–N bond lengths for InGaN alloys are plotted in figure 2a as a function of InN fraction. As expected, the distances for all alloys are close to the average NN bond lengths of InN (2.15 Å) and GaN (1.95 Å), respectively, and show relatively little variation (<5% overall) with composition, whereas, as shown in figure 2b, the weighted mean of the In–N and Ga–N NN bonds varies linearly between those of the binary constituents, in accordance with the MB results [21]. However, when comparing MBE and MOCVD samples of similar InN fraction, we find that the In–N and Ga–N bond lengths are systematically *longer* in the MOCVD samples. We shall refer to the weighted mean of the In–N and Ga–N distances as the average cation–anion distance. For InN-rich MBE samples, the average cation–anion distance coincides with the cation–anion distance predicted by Vegard's law. However, for MBE samples, with InN fractions below 40%, the average cation–anion distance is significantly smaller than that predicted. For comparable InN-poor MOCVD samples, the average cation–anion distance is somewhat closer to the Vegard's law prediction. These incidental effects, due to strain, have no bearing on the matter of phase segregation and will be discussed later.

In all samples the numbers of In and Ga atoms detected by EXAFS in the second coordination sphere were found to be in agreement with those for a random alloy with the In/Ga composition ratio measured by WDX. This result precludes strong clustering of pure InN dots in InGaN alloys. The In–In and In–Ga distances, obtained from In K-edge EXAFS, and the Ga–In and Ga–Ga distances, obtained from Ga K-edge EXAFS, are compared in figure 3. In–Ga and Ga–In distances coincide for InN-rich MBE samples ($x \geq 60\%$), and also for a single MOCVD sample with 40% InN. However, for MBE and MOCVD samples with less than 40% InN, the In–Ga and Ga–In separations differ significantly: *the mean In–Ga distance is consistently larger than the mean Ga–In distance*. This difference in the length of "mixed cation" separations provides a clear indication of a non-random distribution of cations in the sample. In short, this result indicates the existence of InN-rich regions in InN-poor material.

A gross deviation from randomicity in the distribution of cations, leading to different coordination numbers of next-nearest cation neighbours, would indicate the existence of profound clustering or strong phase segregation; this has been found in EXAFS studies of rare earth-doped nitrides [26–28], at impurity concentrations as low as a few atomic per cent. In contrast, such large deviations from the random

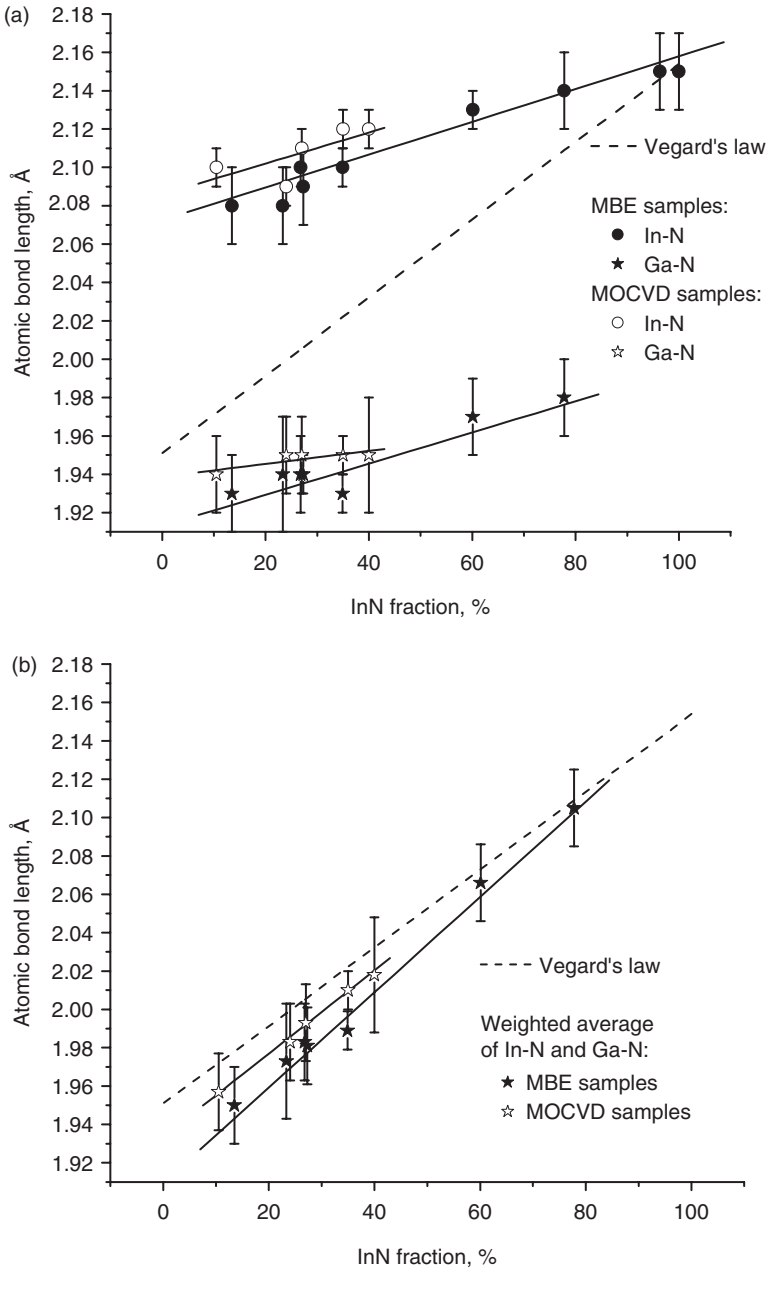

Figure 2. In–N and Ga–N bonds (a) and weighted average of In–N and Ga–N bonds (b) as a function of InN fraction. Solid lines are linear fits to the data.

distribution of cations have not been observed for InGaN epilayer samples in this work. However, EXAFS fits have rather large uncertainties for the coordination number (typically ~15%). For a smaller degree of phase separation, an alloy could not be distinguished from a random alloy in terms of coordination numbers. On the

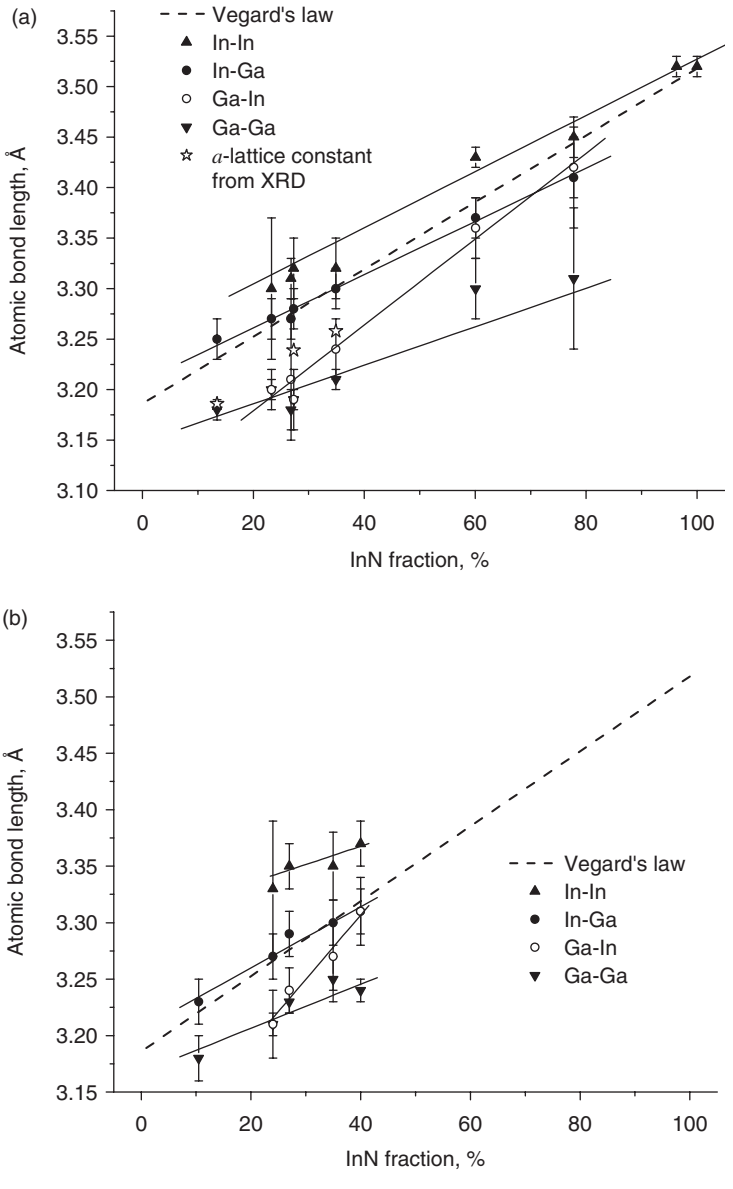

Figure 3. Next-nearest neighbour distances as a function of InN fraction in MBE (a) and MOCVD (b) samples. Solid lines are linear fits to the data.

other hand, the deficit of Ga atoms observed in the average In local structure and the corresponding deficit of In atoms in the average Ga local structure clearly indicates the presence of InN-rich regions (and complementary GaN-rich ones) in our InN-poor samples. Thus, the difference in "mixed cation" distances, reported here, indicates a *weak* phase separation in the form of InN-rich and GaN-rich InGaN regions, which occurs predominantly at rather low InN fractions, $x < 0.4$.

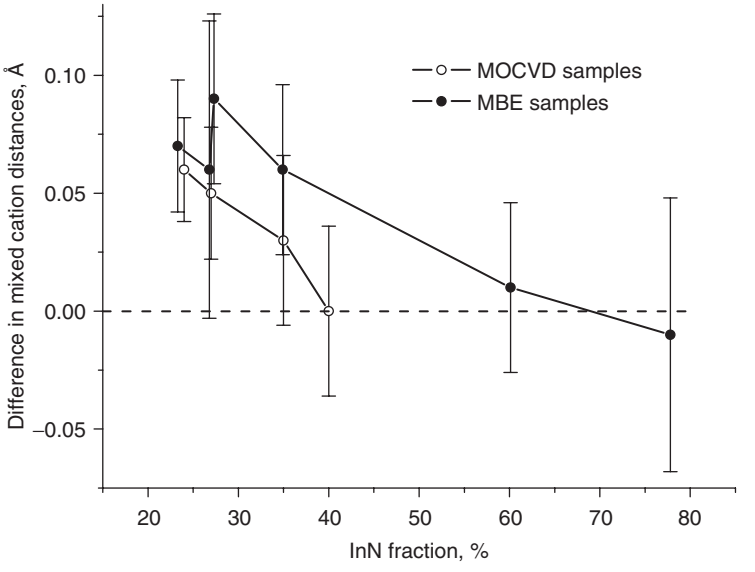

Figure 4. Difference between In–Ga distance of In local structure and Ga–In distance of Ga local structure for MBE and MOCVD samples.

Figure 4 summarizes the NNN data related to the difference in "mixed cation" distances on the In and Ga sublattices as a function of InN content. It clearly shows that the difference in separations, i.e. the degree of non-randomness, *increases* with *decreasing* InN fraction. The disparity is always higher for MBE than for MOCVD samples with the same InN fraction. The largest measured difference of 0.09 Å, corresponding to about 2.8% of the corresponding lattice constant, is observed for an MBE sample with a global InN fraction of ~27%. The trend for all MOCVD samples and for most MBE samples is clearly that of increasing disparity of the Ga and In sublattices with decreasing InN fraction.

Since EXAFS tells us nothing directly about the spatial distribution of different phases, it is important to distinguish the effects of In aggregation from those of random compositional disorder on the local scale: in the case of random compositional disorder, the distribution of cations, of whichever kind, is still *random* and the average local structures of In and Ga will be the same. However in the case of In aggregation, there is a real *difference* in the In and Ga local structures since on average more In atoms are located in InN-rich regions and more Ga atoms in GaN-rich regions; this is completely and trivially true for the totally segregated sample presented in the introduction. For real samples, the situation is also quite clear if we understand the limitations of the EXAFS technique.

3.2. *Relation to optical properties and XRD*

We now attempt to reconcile the local structure results described above with what is already known about the optical properties of the examined samples [29–32]. Firstly, luminescence spectroscopy showed that the peak emission energies of comparable MBE and MOCVD samples were somewhat different: the peak emission energies of

MBE samples are always lower than those of MOCVD samples of similar composition [29]. This fact suggests that a higher degree of indium aggregation in MBE samples, compared to MOCVD samples of the same average composition, produces higher local InN fractions in InN-poor regions, leading to lower emission energies. This clearly links the local structure with the emission properties and solves one mystery.

Next, the Stokes' shift between absorption and emission is largest for samples with an intermediate range of InN content [31, 33, 34], indicating that the highest degree of exciton localization occurs for this most mixed composition. However, the results presented in this letter show that the In and Ga local structure is the same for In-rich MBE samples ($x \geq 60\%$) and for MOCVD InGaN sample with 40% of InN. In these cases, exciton localization can result only from compositional disorder in a random alloy: there is no phase segregation in the InN-rich samples. Random disorder cannot be detected by EXAFS since EXAFS provides an averaged picture of the local structure of a particular atom. Therefore, the results of In and Ga local structure studies by means of EXAFS suggest that in InGaN alloys with InN fraction less than 40% InN, excitons are localized on InN-rich InGaN regions, whereas for InGaN alloys with InN fractions of 40% and more, exciton localization is likely to be due to random compositional disorder only. The appearance of InN-rich regions with *decreasing* InN fraction compares well with the concurrent increase of InGaN emission efficiency [35], suggesting further that InN-rich InGaN regions act as efficient exciton localization and/or emission centres.

Finally, the statistics of phase segregation depends upon both the size and the composition of InN-rich (and corresponding GaN-rich) regions; EXAFS averages local structure configurations and does not distinguish between the two contributions. If, however, the observed difference between the "mixed" cation distances were to equal the difference of 0.36 Å between the lattice constants of InN and GaN, this would indicate a complete phase separation of InGaN into InN and GaN, i.e. in this special case almost all of the In and Ga atoms would be found in InN and GaN phases, respectively. (Equivalently, if the "mixed" cation distances were found to be equal in length, there would be no phase separation). In the singular case of a two-phase mixture of InN quantum boxes and InGaN alloy, a splitting of the metallic shell peak in the Fourier transform of In EXAFS was clearly observed [36].

Consider a separation into only two components by way of illustration. The ratio of the difference in the "mixed" cation bonds to the difference in lattice constants of the binary constituents acts as a metric of the degree of phase segregation in a non-random alloy; it is equal to the fraction, F, of In atoms residing in In-rich regions:

$$F = \frac{d_{\text{In-Ga}} - d_{\text{Ga-In}}}{a_{\text{In-N}} - a_{\text{Ga-N}}}. \tag{3}$$

Considering only a two-component mixture, the following relations can be written for the average InN composition of an alloy, x_{average}:

$$x_{\text{average}} = x_{\text{In-poor}}(1 - f) + x_{\text{In-rich}}\, f, \tag{4}$$

$$f = \frac{F x^{\text{In-poor}}}{(1 - F)x^{\text{In-rich}} + F x^{\text{In-poor}}}, \tag{5}$$

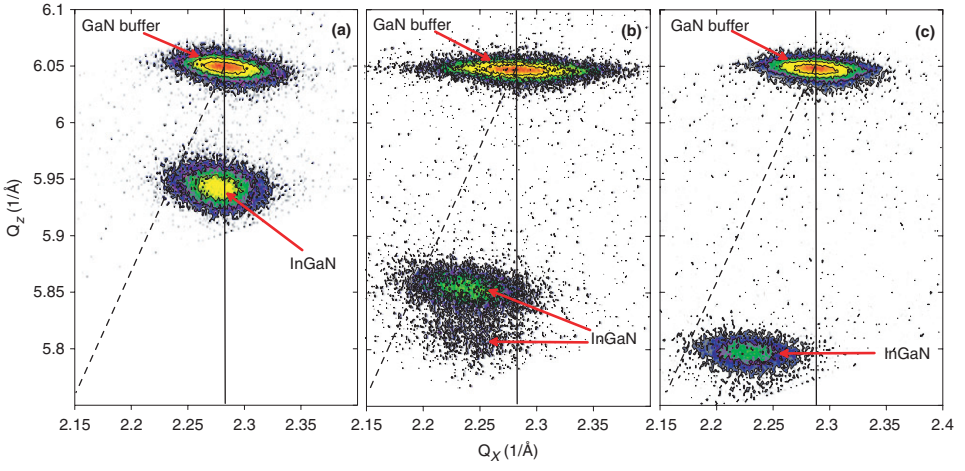

Figure 5. Asymmetric reciprocal space maps of GaN and InGaN (10.5) reflections for MBE-grown samples with InN fraction of 13.5% (a), 27.3% (b) and 34.9% (c). The vertical full lines and the tilted dashed lines indicate coherent growth to the GaN buffer and full relaxation, respectively.

where $x_{\text{In-rich}}$ is the InN content of InN-rich regions, $x_{\text{In-poor}}$ is the InN content averaged over the rest of the material, and f is the filling factor, i.e. the partial volume of the material occupied by the InN-rich regions. Assuming, as an educated guess, that the InN fraction of the InN-rich phase is 10% greater than the average content (x_{average}), for the sample with the highest degree of phase separation ($x = 27\%$) an estimation using equations (3)–(5) shows that In-rich regions (with $x_{\text{In-rich}} \approx 30\%$) occupy ~25% of the total volume of this sample.

In order to compare the short range order probed by EXAFS with long-range order, reciprocal space maps (RSM) were measured by high-resolution XRD of MBE samples with average InN contents of 14%, 27% and 35%, as shown in figure 5. Analysis of the RSMs reveals that the InGaN epilayer with lowest InN content is nearly pseudomorphic (i.e. $a_{\text{InGaN}} = a_{\text{GaN}}$), whereas samples with higher InN content are partially relaxed. For the sample with $x = 27\%$, partial phase segregation is inferred from the two InGaN-related diffraction spots (different c, but the same a lattice constant) which correspond to regions of different InN content. Recall that the difference in "mixed" cation distances of In and Ga local structures obtained from EXAFS analysis (i.e. the degree of phase separation) was highest for this sample. This may suggest that partial phase separation for this sample reaches the (high) degree necessary for its detection by XRD. Calculations based upon elasticity theory [37] estimate the InN fraction of the InN-rich phase to be $x = 31\%$, fortuitously close to the assumed InN content used for illustrative purposes above.

3.3. *Influence of strain on EXAFS and XRD measurements*

The NNN separations determine the lattice constant a of a semiconductor alloy. In a random ternary alloy $A_xB_{1-x}C$ the lattice constant a is the *average* NNN distance.

Since the weighted average of A–A and B–B distances is expected to be close to the length of ''mixed'' cation A–B and B–A bonds, which should be equal in a random alloy, the ''mixed'' cation bond length is in fact the lattice constant a of a random alloy, which depends on the alloy composition x according to Vegard's law:

$$a(\mathrm{A}_x\mathrm{B}_{1-x}\mathrm{C}) = r(\mathrm{A}-\mathrm{B}) = r(\mathrm{B}-\mathrm{A}) = xr(\mathrm{A}-\mathrm{A}) + (1-x)r(\mathrm{B}-\mathrm{B}). \tag{6}$$

In a partially phase-separated alloy the weighted average of ''pure'' cation–cation distances and that of ''mixed'' cation–cation distances are expected to be close to the lattice constant a:

$$a(\mathrm{In}_x\mathrm{Ga}_{1-x}\mathrm{N}) = xr(\mathrm{In}-\mathrm{In}) + (1-x)r(\mathrm{Ga}-\mathrm{Ga}) = xr(\mathrm{In}-\mathrm{Ga}) + (1-x)r(\mathrm{Ga}-\mathrm{In}). \tag{7}$$

In the case of dilute InGaN samples with InN fraction less than 15%, for which no In atoms could be fitted to EXAFS of the second coordination sphere, the weighted average of In–Ga and Ga–Ga distances is expected to be close to the lattice constant a:

$$a(\mathrm{In}_x\mathrm{Ga}_{1-x}\mathrm{N}) = xr(\mathrm{In}-\mathrm{Ga}) + (1-x)r(\mathrm{Ga}-\mathrm{Ga}). \tag{8}$$

The lattice constants a calculated from NNN distances by equations (6)–(8) are shown in figure 6. In the case of samples with In-rich and Ga-rich regions the weighted average of ''pure'' cation–cation bonds or that of ''mixed'' cation–cation bonds (whichever had smaller fitting errors) was taken to approximate the a lattice constant. The a lattice constants obtained by XRD are shown in figure 6a for comparison. The agreement between EXAFS and XRD is seen to be very good.

For MBE samples the behaviour of the a lattice constant obtained from NNN distances mirrors that of the NN In–N and Ga–N bond lengths described previously. Since Vegard's law does not take into account the strain state of epilayers, such biaxial strain is likely to be the cause of the shrinkage of both NN and NNN distances observed in our samples. The existence of biaxial compressive strain is confirmed by XRD, as shown in figure 5. For MOCVD samples, NNN distances shrink due to the strain when the InN fraction exceeds 24%. The strain does not, however, affect NN bond lengths in these samples. We conclude that MBE samples with InN fraction less than 40% and MOCVD samples with InN fraction less than 25% are subjected to compressive strain which is higher in MBE samples than in MOCVD ones of the same InN content, whereas the set of In-rich MBE samples is essentially relaxed, due to the extremely large lattice mismatch: the critical thicknesses of InN-rich alloys grown directly on sapphire are close to zero. The case of MBE samples where both NN and NNN distances shrink suggests that compressive strain in the epilayers, imposed by the GaN substrates, is accommodated through both angle and length distortion of cation-anion bonds. NN bonds remain almost unaffected when NNN distances shrink due to strain in MOCVD samples: it is easier to bend bonds than to stretch them, in agreement with theoretical calculations [38].

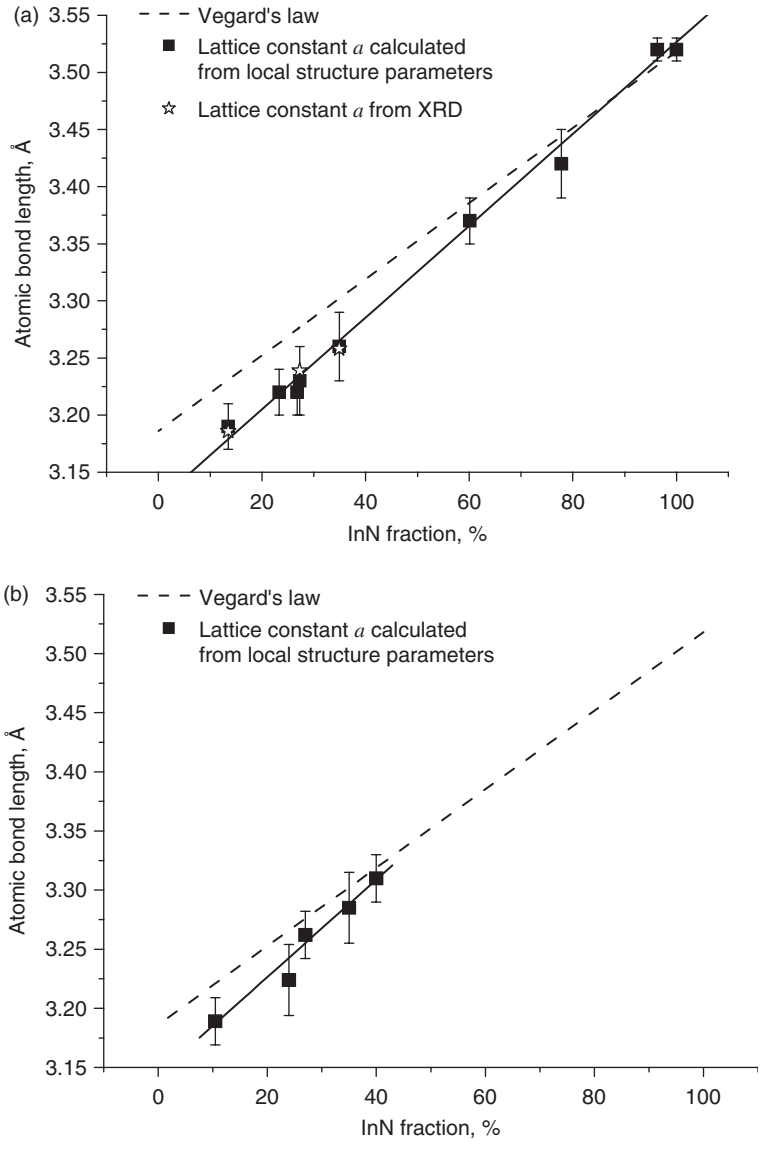

Figure 6. The dependence of the lattice constant, a, calculated from In and Ga local structure parameters, on InN fraction for MBE (a) and MOCVD (b) samples. Solid lines are linear fits to the data.

3.4. *Excitation–emission efficiency and localization on a non-random lattice*

The concluding section of our discussion treats in a somewhat speculative manner possible connections between weak localization, as related to the weak phase segregation reported above, and strong localization, related to accidental QD formation, in InGaN alloys.

The starting point of the discussion is the excitation–emission model that was put forward previously [3, 4]. We suppose that photonic or electronic excitation interacts with *de*localized excitons in the (weakly) phase-separated alloy InGaN. Luminescence, as always, is related to exciton localization: if an exciton cannot delocalize within a characteristic lifetime, the consequence is a luminescence event (emission of a photon). Crudely speaking, the delocalized exciton is an excitation of the GaN-rich sublattice, whereas localized excitons favour the InN-rich sublattice. Energy delocalization after localization may be called back-transfer of excitation (from localized to delocalized states). This leads to a decrease in luminescence output if the back-transferred excitation becomes shunted somehow into a non-radiative branch.

The correlation of energy with composition in an alloy leads to an intimate connection between spatial and energy (and therefore momentum) localization of excitons. In order to assign a definite energy to an exciton, we suppose that it has a finite extent and normalizes the portion of lattice with which it interacts; essentially it 'samples' the In/Ga ratio within its volume (another bottom-up method). While it is clear that delocalized excitons have in general rather higher energy than localized ones, it is difficult to know exactly what this means physically. There is a world of difference between a Wannier and a Frenkel exciton. The mean difference in energy between the peak of the emission and the edge of the excitation spectrum is Stokes' shift.

Luminescence efficiency measures the ratio of the photon emission rate to the total rate of annihilation of delocalized excitons, regarded as quanta of the excitation. For the efficiency to attain its maximum value of unity, (i) excitation must preferentially reach emitting centres (whatever their nature) rather than non-radiative traps and (ii) back-transfer of excitation from emitting centres to delocalized states must be eliminated.

For the first point, we note that the migration of excitation through a lattice is enhanced by percolation. We speculate that the complementarity of the Ga and In sublattices enhances the delivery of excitation to lumophores when the InN fraction is lower than the percolation threshold. By the same token, excitons localized on InN-rich regions of the lattice will not readily delocalize. Although the movement of excitons through an energy-disordered environment cannot be described simply as hopping of classical particles between lattice points, it may be significant that the percolation threshold defined in this way for the diamond lattice is 0.43, which corresponds approximately to the InN fraction separating random from non-random InGaN alloys. (Of course this may also say something about the formation of the alloy itself during growth: it is notable that no MOCVD material with $x > 0.4$ has been reported in the literature.) As for the second point, transfer of excitation, whether forwards or backwards in energy terms, depends strongly upon the distances involved, whether the mechanism is dipole–dipole ($\sim r^{-6}$) or via tunnelling (exponential). In this context we note that the mean forward-transfer distance (Ga–In) is shorter than the back-transfer distance (In–Ga) in strongly luminescent alloys. In this way a small symmetry breaking can have profound consequences. Finally, we call attention to recent results, also not yet well understood, related to the ferromagnetism of GaN doped with Gd [39]: in this system too the effects of percolation (of spins) appear to increase as the impurity becomes more dilute.

4. Conclusions

In summary, a difference between In and Ga local structures was observed by EXAFS investigations of certain InGaN epilayers and attributed to weak phase segregation into InN-rich and GaN-rich regions. An estimate of the extent of these regions can be made, with the simplest set of assumptions, but EXAFS provides no information about the spatial distribution or size of InN-rich regions. Remarkably, the degree of the phase separation was found to *increase* with *decreasing* InN fraction x in $In_xGa_{1-x}N$. This observation correlates with a concurrent increase of luminescence efficiency, suggesting that *slightly* InN-rich clusters are responsible for efficient exciton localization and recombination in InGaN light-emitting devices. However, the (possibly spontaneous) formation of InN-richer regions in InN-poorer material remains to be explained in a fundamental way on the basis of an improved understanding of the growth thermodynamics of InGaN alloy.

Acknowledgements

The authors are grateful to Dr JFW Mosselmans for leading the InGaN EXAFS programme at SRS Daresbury Laboratory, to Dr Benjamin Hourahine for useful discussions, and to Professor Yasushi Nanishi, Professor Enrique Calleja, Dr Ian M. Watson and Dr Wim van der Stricht for providing the samples used in this study. V. Kachkanov acknowledges financial support from the Overseas Research Students Award Scheme, Strathclyde University and Daresbury Laboratory.

References

[1] I.H. Ho and G.B. Stringfellow, Appl. Phys. Lett. **69** 2701 (1996).
[2] B. Gil (Editor), *Low-dimensional Nitride Semiconductors*, 1st ed. (Oxford University Press, Oxford, 2002).
[3] K.P. O'Donnell, R.W. Martin and P.G. Middleton, Phys. Rev. Lett. **82** 237 (1999).
[4] R.W. Martin, P.G. Middleton, K.P. O'Donnell, *et al*., Appl. Phys. Lett. **74** 263 (1999).
[5] S. Chichibu, T. Azuhata, T. Sota, *et al*., Appl. Phys. Lett. **69** 4188 (1996).
[6] T. Narukawa, Y. Kawakami, M. Funato, *et al*., Appl. Phys. Lett. **70** 981 (1997).
[7] V.Yu. Davydov, A.A. Klochikhin, V.V. Emtsev, *et al*., Phys. Stat. Sol. (b) **234** 787 (2002).
[8] K. Okamoto, A. Kaneta, Y. Kawakami, *et al*., J. Appl. Phys. **98** 064503 (2005).
[9] T.M. Smeeton, M.J. Kappers, J.S. Barnard, *et al*., Appl. Phys. Lett. **83** 5419 (2003).
[10] T.E. Li, E. Hahn, D. Gerthsen, *et al*., Appl. Phys. Lett. **86** 241911-1 (2005).
[11] S.-W. Feng, E.-C. Lin, T.-Y. Tang, *et al*., Appl. Phys. Lett. **83** 3906 (2003).
[12] H.J. Chang, C.H. Chen, Y.F. Chen, *et al*., Appl. Phys. Lett. **86** 021911-1 (2005).
[13] S. Srinivasan, F. Bertram, A. Bell, *et al*., Appl. Phys. Lett. **80** 550 (2002).
[14] K.P. O'Donnell, J.F.W. Mosselmans, R.W. Martin, *et al*., J. Phys. C **13** 6977 (2001).
[15] S. Pereira, M.R. Correia, E. Pereira, *et al*., Appl. Phys. Lett. **79** 1432 (2001).
[16] S. Pereira, M.R. Correia, E. Pereira, *et al*., Appl. Phys. Lett. **81** 1207 (2002).
[17] Y.-H. Cho, G.H. Gainer, A.J. Fischer, *et al*., Appl. Phys. Lett. **73** 1370 (1998).

[18] S.J. Gurman, J. Synchrotron Radiat. **2** 56 (1995).
[19] R.W. Martin, P.R. Edwards, K.P. O'Donnell, *et al.*, Phys. Stat. Sol. (a) **192** 117 (2002).
[20] A.V. Blant, T.S. Cheng, N.J. Jeffs, *et al.*, Mater. Sci. Eng. B **50** 38 (1997).
[21] J.C. Mikkelsen and J.B. Boyce, Phys. Rev. B **28** 7130 (1983).
[22] J.L. Martins and A. Zunger, Phys. Rev. B **30** 6217 (1984).
[23] Z. Wu, K. Lu, Y. Wang, *et al.*, Phys. Rev. B **48** 8694 (1993).
[24] A. Balzarotti, M. Czyzyk, A. Kisiel, *et al.*, Phys. Rev. B **30** 2295 (1984).
[25] W.-F. Pong, R.A. Mayanovic, B.A. Bunker, *et al.*, Phys. Rev. B **41** 8440 (1990).
[26] V. Katchkanov, J.F.W. Mosselmans, S. Dalmasso, *et al.*, Superlattices Microstruct. **36** 729 (2004).
[27] V. Katchkanov, J.F.W. Mosselmans, S. Dalmasso, *et al.*, Mat. Res. Soc. Symp. Proc. **798** Y5.10.1 (2004).
[28] V. Katchkanov, J.F.W. Mosselmans, K.P. O'Donnell, *et al.*, Opt. Mater. **28** 785 (2006).
[29] I. Fernandez-Torrente, D. Amabile, R.W. Martin, *et al.*, Mat. Res. Soc. Symp. Proc. **798** 673 (2003).
[30] K.P. O'Donnell, I. Fernandez-Torrente, P.R. Edwards, *et al.*, J. Cryst. Growth **269** 100 (2004).
[31] R.W. Martin, P.R. Edwards, S. Hernandez, *et al.*, Mat. Res. Soc. Symp. Proc. **831** E3.6 (2005).
[32] S. Hernández, R. Cuscó, D. Pastor, *et al.*, J. Appl. Phys. **98** 013511-1 (2005).
[33] M. Kurouchi, T. Araki, H. Naoi, *et al.*, Phys. Stat. Sol. (b) **241** 2843 (2004).
[34] J. Wu, W. Walukiewicz, K.M. Yu, *et al.*, Solid St. Commun. **127** 411 (2003).
[35] T. Mukai, IEEE J. Sel. Top. Quantum. Electron. **8** 264 (2002).
[36] K.P. O'Donnell, M.E. White, S. Pereira, *et al.*, Mater. Sci. Eng. B **93** 150 (2002).
[37] S. Pereira, M.R. Correia, E. Pereira, *et al.*, Appl. Phys. Lett. **80** 3913 (2002).
[38] K. Kim, W.R.L. Lambrecht and B. Segall, Phys. Rev. B **53** 16310 (1996).
[39] S. Dhar, L. Pérez, O. Brandt, *et al.*, Phys. Rev. B **72** 245203 (2005).